OPEN

Magnetic-assisted triboelectric nanogenerators as self-powered visualized omnidirectional tilt sensing system

Mengdi Han, Xiao-Sheng Zhang, Xuming Sun, Bo Meng, Wen Liu & Haixia Zhang

National Key Lab of Nano/Micro Fabrication Technology, Institute of Microelectronics, Peking University, Beijing, China, 100871.

The triboelectric nanogenerator (TENG) is a promising device in energy harvesting and self-powered sensing. In this work, we demonstrate a magnetic-assisted TENG, utilizing the magnetic force for electric generation. Maximum power density of 541.1 mW/m^2 is obtained at 16.67 MΩ for the triboelectric part, while the electromagnetic part can provide power density of 649.4 mW/m^2 at 16 Ω. Through theoretical calculation and experimental measurement, linear relationship between the tilt angle and output voltage at large angles is observed. On this basis, a self-powered omnidirectional tilt sensor is realized by two magnetic-assisted TENGs, which can measure the magnitude and direction of the tilt angle at the same time. For visualized sensing of the tilt angle, a sensing system is established, which is portable, intuitive, and self-powered. This visualized system greatly simplifies the measure process, and promotes the development of self-powered systems.

W ith the rapid development of microelectronic technology, personal electronics and wireless sensors are becoming widely used. However, traditional power supply methods, such as wires and batteries, cannot meet the need of portability and long lifetime. By contrast, harvesting energy from the ambient environment is a promising way to power the microelectronic devices[1,2]. Based on electromagnetic[3,4], piezo-electric[5–7], and electrostatic[8,9] transduction mechanisms, numerous generators have been fabricated to convert mechanical energy in to electricity. Moreover, triboelectric nanogenerators (TENGs), which couples the triboe-lectrification and electrostatic induction, have been proposed and studied very recently[10,11]. Due to the high output performance[12], various enhancing method[13,14], and wide material selection[15,16], TENGs have been suc-cessfully utilized in personal electronics[17], biomedical systems[18], electrochemical applications and human body energy harvesting[19]. In addition, TENGs as self-powered active mechanical and chemical sensors[20,21] have also been demonstrated.

Generally, there are three types of TENG: vertical contact-separation type[12,22], in-plane sliding type[23,24], and single-electrode type[25,26]. For each type, high open-circuit voltage (several hundred volts) can be easily achieved, which is beneficial in the applications requiring high voltages. However, short-circuit current of the TENGs is relatively low (usually less than a few milliamps), which limits their applications. Combining two or more energy conversion mechanisms together is an effective way to compensate the low short-circuit current of TENGs. Devices combining piezoelectric nanogenerator[27,28], pyroelectric nanogenerator[29] *etc.* with a TENG have been investigated and shown enhanced performance.

In this work, we developed a magnetic-assisted TENG to convert mechanical energy into electricity. The magnets in the TENG have two important roles. The first is to provide magnetic repulsive force, which is essential for the separation between two friction materials. The second is to induce voltage in the specially designed copper electrodes, thus combining electromagnetic output together with the TENG. Output characterization of the triboelectric part and the electromagnetic part has been conducted systematically, indicating that both large voltage and large current can be obtained in this TENG. Moreover, replacing traditional mechanical restoring force with the magnetic force effectively prevent the TENG from mechanical fatigue. The magnetic-assisted TENG was also demonstrated as a self-powered active omnidirectional tilt sensor. Large tilt angles can be measured in all directions and a visualized self-powered system was built to intuitively reflect the change of tilt angle.

Results

Structure of the magnetic-assisted TENG. Structure of the magnetic-assisted TENG is shown in Figure 1a, which includes the top steel mass with the weight of 18.0 g, top NdFeB permanent magnet with the radius of 9.5 mm and the height of 1.5 mm, silica layer, spiral-shaped electrode wrapped by polyimide, and the bottom NdFeB permanent magnet with the radius of 5.0 mm and the height of 0.5 mm. Each part is located inside a polytetrafluoroethene (PTFE) cylinder. The magnets are Nickel-plated to avoid being corroded. The top magnet also serves as the top electrode of the TENG and has an opposite polarity with the bottom magnet, thus providing a magnetic repulsive force. Silica was coated onto the top magnet as a friction material. To convert mechanical energy into electricity in both triboelectric and electromagnetic mechanisms, the bottom copper electrode was fabricated as spiral shape, forming a coil to generated electricity based on Faraday's law. Polyimide was then fabricated around the spiral-shaped copper electrode as another friction material. To enhance the triboelectric output, nanostructures were created on the polyimide surface using inductively coupled plasma (ICP). Photograph of the whole TENG is shown in Figure 1b. The fabricated TENG is cylindrical with the diameter of 2.4 cm and the height of 2.0 cm. Photograph and scanning electron microscopy (SEM) image of the spiral-shaped copper electrode are shown in Figure 1c, d. The width, height and spacing of the spiral are 150 µm, 18 µm, and 150 µm, respectively. SEM image of nanostructures on polyimide surface are shown in Figure 1e.

Working principle. Working principle of the magnetic-assisted TENG can be divided into two parts: the triboelectric part and the electromagnetic part. Current flow generated in the triboelectric part is caused by the coupling between the triboelectric effect and electrostatic induction. According to the triboelectric series[30], the silica surface will be positively charged while the polyimide surface is with negative charges after cycles of contact and separation of the two materials. In this case, if the top and bottom electrodes are connected, charges will redistribute on both electrodes due to the electrostatic induction. Then, as shown in Figure 2a<i>, given an external force, the gap distance decreases, leading to increased electric field (E) between the top and bottom plates. To balance the electric field, electrons will flow from the top electrode to the bottom electrode. When the external force is removed, the magnetic repulsive force will push the top plate to the original position, as shown in Figure 2a<ii>. This brings about the decrease of electric field, in which case a reversed current flow is produced. To verify the change of electric field, finite element method (FEM) simulations were conducted in COMSOL software package. A 2D axisymmetric model

was established and the electric potential at infinite was set as zero. Charge densities on the friction surfaces were set as 5 µC/m² and −5 µC/m², respectively. By changing the gap distance, different electric field distribution is achieved as shown in Figure 2b, which is consistent with the analyzed working process.

Current flow of the electromagnetic part is caused by the electromagnetic induction. As shown in Figure 2c<i>, when applying an external force, the magnetic flux (Φ_B) increases with the decreasing of gap distance, thus inducing current flow in the spiral-shaped electrode. Then, by removing the external force, magnetic force makes the gap distance increase, as shown in Figure 2c<ii>. In this case, magnetic flux decreases, causing a reversed current flow in the spiral-shaped electrode. Correspondingly, FEM simulations about the magnetic flux density distribution were carried out. The geometry was also 2D axisymmetric with zero magnetic scalar potential at infinite. In this model, relative permeability of the magnetic material (*i.e.*, NdFeB) was set as 1.044. Magnetization of the top and bottom magnet was set as −838000 A/m and 838000 A/m in Z-direction, respectively. As shown in Figure 2d, when the gap distance decreases, large magnetic flux density is obtained.

Output characterization. The output performance of the magnetic-assisted TENG was measured with a 5 Hz external force. As shown in Figure 3a, with a 100 MΩ probe, output voltage of the TENG reaches to 90 V. By connecting a 100 kΩ external resistance parallel to the TENG, output current is recorded with a peak value of 6 µA, as shown in Figure 3b. Based on the theoretical calculation[22], the output curve of TENGs is dependent on the external resistance. The external resistance will not only affect the peak shape, but also influence the output value. Therefore, to further characterize the output performance of the TENG, output voltages under different external loads were investigated. As shown in Figure 3c, peak output voltage raises with the increasing value of the external loads, and the growth rate slows down at high resistance. As a result, peak output power reaches maximum at 16.67 MΩ, with the value of 170 µW. Besides the triboelectric output, the movement of the magnet will induce voltage in the spiral-shaped copper electrode. The induced voltage was first measured with a 1 MΩ probe. As shown in Figure 3d, peak voltage of 71.86 mV is achieved in the electromagnetic part. Compared with the triboelectric output, voltage generated by the electromagnetic induction is relatively low. However, large current can be obtained thanks to the low resistance between the two ends of the spiral. The induced current was then measured with a 0.5 Ω external resistance and peak current of 12.66 mA is achieved as shown in Figure 3e. Since the inner resistance of the electromagnetic part is low, good output
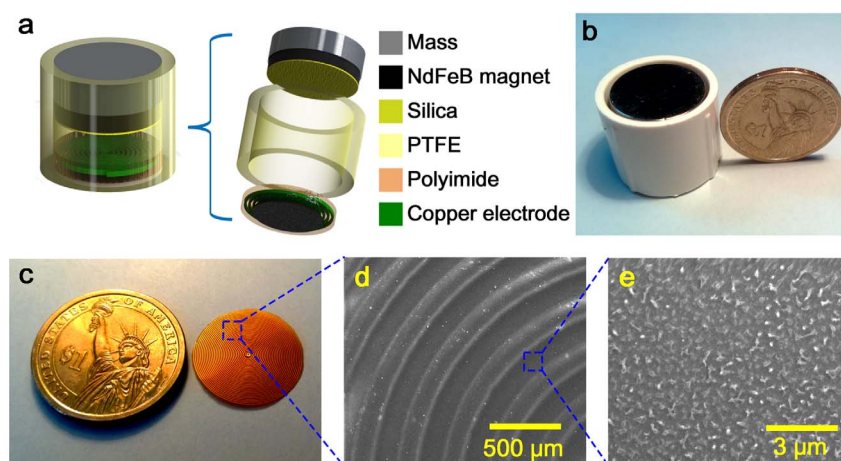

Figure 1 | Structure of the magnetic-assisted TENG. (a) Schematic diagram and (b) photo of the magnetic-assisted TENG. (c) photo and (d) SEM image of the spiral-shaped copper electrode. (e) SEM image of the nanostructures on the polyimide surface.
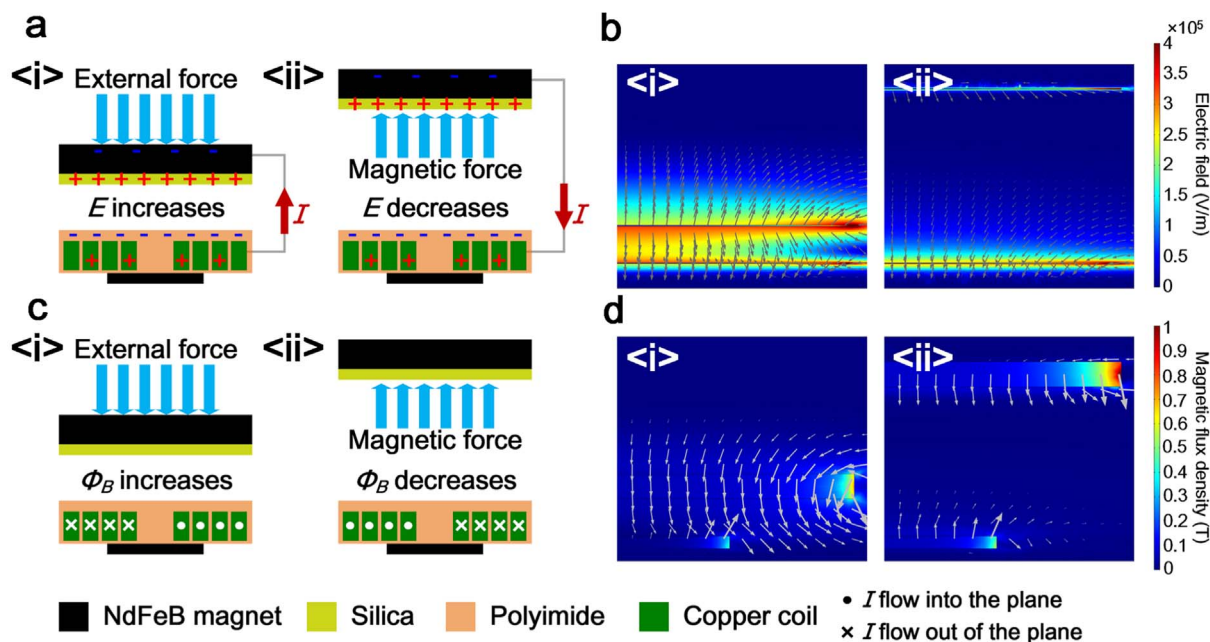
Figure 2 | Working mechanism of the magnetic-assisted TENG. (a) Schematics of the triboelectric output, indicating the relationship between gap distance, electric field, and current flow direction. (b) FEM simulation of the electric field with different gap distances. (c) Schematics of the electromagnetic output, indicating the relationship between gap distance, magnetic flux, and current flow direction. (d) FEM simulation of the magnetic flux density with different gap distances.

performance can be achieved at very low resistances even below 10 Ω. As verified in Figure 3f, the output voltage increases dramatically as the load resistance varies from 0 to 32 Ω, and remains almost unchanged at higher resistance. Maximum peak power of 204 µW is obtained at 16 Ω, indicating low optimized resistance of the electromagnetic part.

TENG as a self-powered omnidirectional tilt sensor. In the separation process of two friction surfaces, gravity of the mass is used to balance the magnetic repulsive force. By reducing the radius and height of top magnet to 5.0 mm and 0.5 mm, the magnetic repulsive force can be reduced. Furthermore, we increase the weight of top mass to 36.0 g and the gravity can balance the magnetic force at a
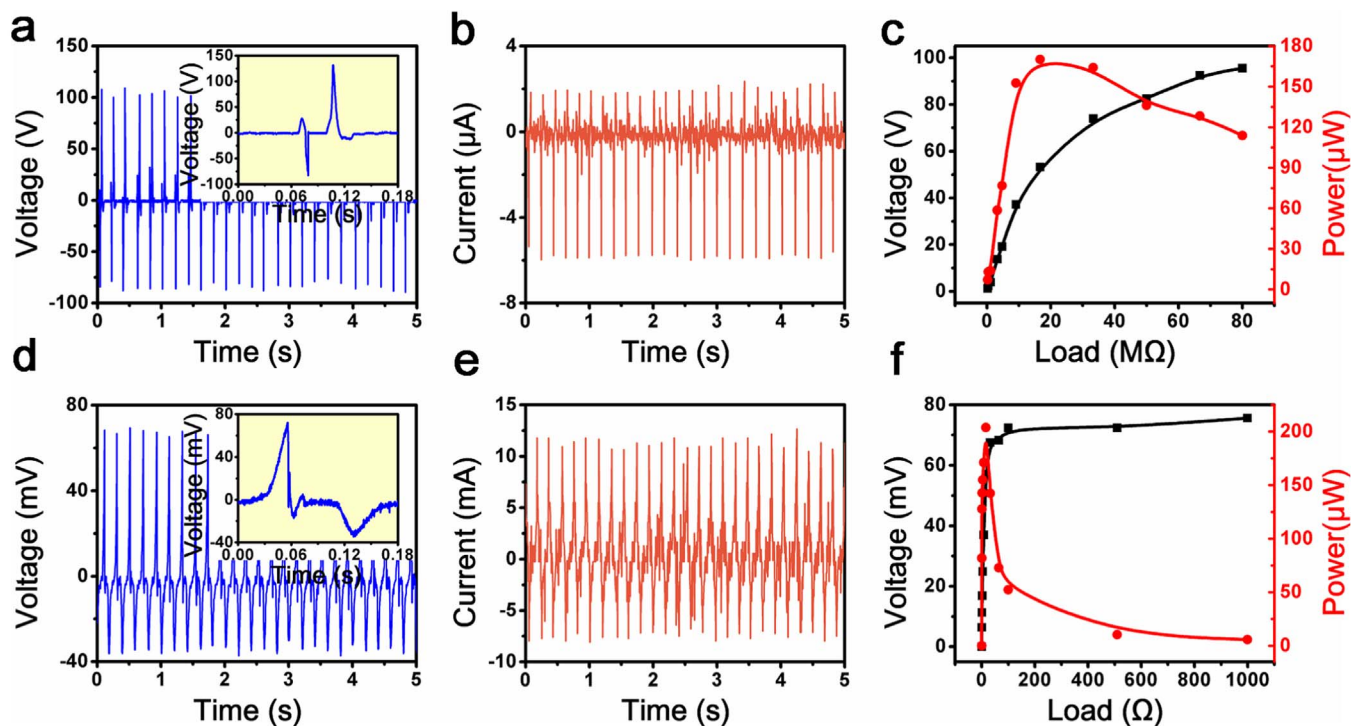

Figure 3 | Output performance of the magnetic-assisted TENG. (a) Output voltage and (b) current of the triboelectric part. (c) Triboelectric peak voltage and power under different external load resistances. (d) Output voltage and (e) current of the electromagnetic part. (f) Electromagnetic peak voltage and power under different external load resistances.
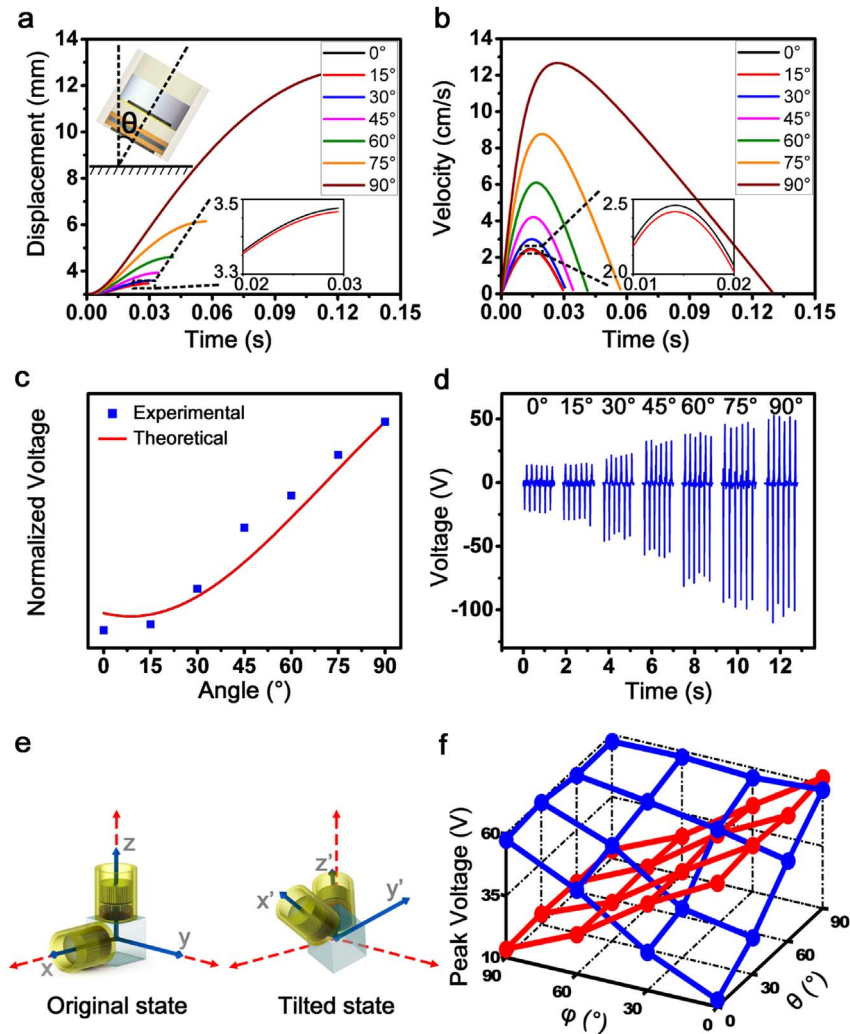
Figure 4 | Demonstration of the magnetic-assisted TENG as a self-powered tilt sensor. Theoretical analysis of (a) time domain displacement and (b) velocity in the separation process under different tilt angles. (c) Comparison of the theoretical and experimental output peak voltage. (d) Measured time domain output voltage at different tilt angles. (e) Schematic diagram of the omnidirectional tilt sensor. (f) Output peak voltage of the two TENGs at 16 different tilt angles.

very short distance. When the TENG is inclined, influence of the mass gravity will be weakened, thus enhancing the separation speed and distance. The contribution of the magnetic force ($F_M(z)$) and gravity along the motion path ($G(\theta)$) can be expressed as[31]:

$$F_M(z) = \frac{\pi\mu_0}{4} M^2 R^4 \left[\frac{1}{z^2} + \frac{1}{(z+2H)^2} - \frac{2}{(z+2H)^2} \right], \quad (1)$$

$$G(\theta) = mg\cos(\theta) + \mu mg \sin(\theta), \quad (2)$$

where μ_0 is the vacuum permeability, M is the magnetization of the magnet, R and H are the radius and height of the cylindrical magnet, z is the distance between two magnet, m is the value of top mass, g is the acceleration of gravity, θ is the tilt angle of the TENG, and μ is the friction coefficient between the mass and PTFE cylinder. Based on the above equations, the displacement and speed of the moving mass versus time can be calculated through a Simulink model. When the tilt angle increases, gravity component reduces, which leads to the increment of maximum displacement. As shown in Figure 4a, the maximum displacement increases from 3.48 mm to 12.71 mm as the tilt angle changes from $0°$ to $90°$. The time required to reach the maximum displacement also increases with the tilt angle. Due to the distance-dependent magnetic force, velocity of the moving mass reaches maximum at a certain position. Figure 4b shows the

velocity-time curve at different tilt angles, indicating that larger tilt angle contributes to faster movement.

Based on the theoretical study of the contact-mode TENG[22], relative movement between the two friction surface (i.e., the movement of the top mass) will affect the output performance of TENGs. A differential equation of the transferred charges can be expressed as:

$$\frac{\partial \Delta Q(t)}{\partial t} = \frac{[Q_0 - \Delta Q(t)]D(t)}{A\varepsilon_0 R_L} - \frac{\Delta Q(t)d_1}{A\varepsilon_1\varepsilon_0 R_L} - \frac{\Delta Q(t)d_2}{A\varepsilon_2\varepsilon_0 R_L}, \quad (3)$$

where ΔQ is the transferred charges, Q_0 is the charges on the friction surface, $D(t)$ is the movement equation, A is the area of the friction surface, R_L is the external load resistance, ε_0 is the vacuum permittivity, ε_i and d_i ($i = 1, 2$) are the relative permittivity and thickness of the two friction materials, respectively. Based on Equation (3), time domain output current can also be obtained from the Simulink model. In addition, by varying the tilt angle, $D(t)$ will be changed thus affecting the output.

To demonstrate the magnetic-assisted TENG as a self-powered omnidirectional tilt sensor, output measurement under different tilt angles was first conducted. As shown in Figure 4c, normalized separation peak voltage versus tilt angle is investigated both experimentally and theoretically. When the tilt angle is small (i.e., less than $30°$), the peak voltage shows no significant change, due to the basically

unchanged separation velocity. As the tilt angle increases (*i.e.*, from 30° to 90°), the peak voltage raises and shows a nearly linear relationship with the tilt angle. The measured time domain output voltage is shown in Figure 4d.

For omnidirectional sensing, two TENGs perpendicular to each other were mounted to a cube. As illustrated in Figure 4e, in the original state, the tilt angles of the two TENGs are 0° and 90°, respectively. With an arbitrary incline (*i.e.*, tilted state in Figure 4e), the tilt angles of the two TENGs will be changed, thus affecting their output voltages. An arbitrary tilt angle can be divided into two parts: rotating θ around X-axis, and rotating φ around Y-axis. Then the tilt angles of the two TENGs (*i.e.*, TA_1 and TA_2) can be expressed as:

$$TA_1 = \arccos(\cos(\theta)\cos(\varphi)), \quad (4)$$

$$TA_2 = 90° - \varphi. \quad (5)$$

A plot demonstrating the relationship between TA_1, TA_2 and θ, φ is shown in Figure S1 in the Supporting Information. By recording the output voltages of two TENGs, TA_1 and TA_2 can be estimated. On this basis, the value of θ and φ can be obtained to determine the specific tilt angle. Experimental measurement was conducted under 16 tilt angles in different directions (both θ and φ vary from 0° to 90°), as shown in Figure 4f and Figure S2. In this way, both the magnitude and direction of the tilt angle can be obtained in this self-powered tilt sensor.

Self-powered visualized system. In addition, a self-powered system based on this magnetic-assisted TENG was built for visual display (see Video S1). As shown in Figure 5a, the TENG was mounted to a slope. A height adjuster was used to change the tilt angle. The output voltage of the TENG is divided thorough a 5 MΩ resistor and then rectified through a diode, keeping only the voltage at the separation process. The half-wave rectified voltage was then utilized to power a LCD-based visual sensor, as shown in Figure 5b. At different tilt angles, the voltage applied to the LCD-based visual sensor changes, thus affecting the final display of the LCD. As shown in Figure 5c, when operating at the tilt angle of 60°, only the first square displays in the LCD screen. Then, as the tilt angle increases to 70° and 80°, the second and third squares in the LCD screen become visible. This self-powered system directly converts the tilt angle information to visual display, without the need to record and analyze the output signal. Therefore, complex measurement device can be removed, which makes the self-powered system totally electric-free. The demonstrated visualized system greatly promotes the development of self-powered system and shows potential applications in the field of self-powered intuitive sensing.

Discussion

This magnetic-assisted TENG has a wider working range against the load resistance compared with previous TENGs, as plotted in Figure S3 in the Supporting Information. When the external load is at MΩ level, the triboelectric part can provide considerable power output. As the load resistance drops to tens of ohms, power output of the triboelectric part decreases nearly to zero. Drastically reduced power output is a common problem for traditional TENGs. In this magnetic-assisted TENG, the moving magnet and spiral-shaped electrode contribute to electromagnetic output, which broadens the application field of the TENG at low resistances. In addition, in the working process, the restoring force is provided by two permanent magnets instead of traditional mechanical structures such as springs or cantilevers. The magnetic repulsive force is accurate and stable, which is not affected by the mechanical fatigue. Stability of the TENG was measured with a 5 Hz periodic external force. Detailed stability measurement is shown in Figure S4 in the Supporting Information.

Compared with other tilt sensors based on electrolysis[32], induction[33] and optics[34], this triboelectric-based self-powered tilt sensor has the following advantages. Firstly, structure of this tilt sensor is simple, without the complicated fabrication process and liquid environment. Secondly, high resolution of about 400 mV per 1° is achieved due to the high output voltage of the TENG. The high output voltage also makes this tilt sensor not easily affected by the noise signal. Thirdly, tilt angle as large as 90° can be measured in all directions thanks to the two mutually perpendicular TENGs. Finally, the tilt sensor is self-powered without any external power supply, which is energy-saving and can be applied in remote areas and emergency power outage situations.

In summary, we present a magnetic-assisted TENG and demonstrate it as a self-powered visualized omnidirectional tilt sensing system. The specially designed spiral-shaped electrode enables this TENG to generate electricity through both triboelectric and electromagnetic mechanisms, with the peak power densities of 541.1 mW/m² and 649.4 mW/m², respectively. Moreover, this TENG can work at a wide range against the load resistance thanks to the output of the electromagnetic part. By carefully controlling the mass and magnetic force, the TENG can be used as a self-powered tilt sensor, with a high resolution of 400 mV per 1°. Theoretical calculation and
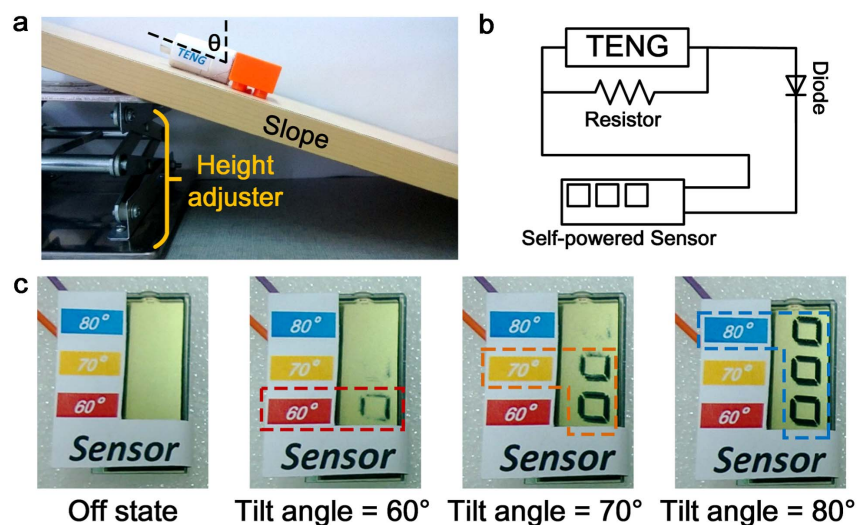

Figure 5 | Demonstration of the visualized tilt sensing system. (a) Measurement system of the self-powered sensor. (b) Electric circuit of the self-powered visible system. (c) Photos of the self-powered visible sensor at different operation states.

experimental measurement of the output voltage at different tilt angles are conducted and shows good consistency. In addition, omnidirectional tilt sensing is realized by two TENGs fixed perpendicular to each other. For visualized sensing, a self-powered system is established based on the LCD screen. This self-powered visualized system eliminates the complicated measure process, and brings great opportunity for the further development of self-powered systems.

Methods

Fabrication of the polyimide wrapped copper electrode. Fabrication of the poyimide wrpped copper electrode was conducted using a polyimide substrate with copper foils on both sides (Figure S5a). Copper was then electroplated on both sides with the thickness of 18 μm (Figure S5b). Next, photoresist was spin coated and patterned on both sides (Figure S5c). Later, the electroplated copper on both sides was wet etched by $FeCl_3$ (Figure S5d). After removing the photoresist (Figure S5e), another layer of polyimide was coated on both sides as the insulate layer (Figure S5f).

Fabrication of the nanostructures on polyimide substrate. Nanostructures on the polyimide substrate was created using ICP. O_2 with a flow rate of 10 sccm was introduced to the chamber. Power of 400 W and 100 W was set to generate and accelerate the plasma ions. After 600 s, nanostructures were fabricated on the polyimide substrate.

Measurement of the TENG. To measure the triboelectric output voltage, a 100× probe (HP9258) was conneceted to the oscilloscope (Agilent DSO-X 2014A). The equivalent internal resistance is 100 MΩ and the corresponding settings in the oscilloscope was adjusted to 100×. To measure the triboelectric output current, a 100 kΩ external resistance was connected parallel to the TENG and the measured signal was calculated to the current value. In the electromagnetic part, 1 MΩ probe was used to measure the voltage and a 0.5 Ω external resistance was parallel connected to measure the current.

Simulink model. The Simulink model includes two parts: mechanical part, and electrical part. The mechanical part is established to obtain the time domain movement equation of the TENG based on the distance-dependent magnetic force. Considering the magnetic repulsive force, gravity, and the friction force, the total acceleration applied to the top mass of TENG can be expressed as:

$$a = F_M(z) - G(\theta),$$

where a is the acceleration, $F_M(z)$ and $G(\theta)$ has been expressed in equation (1) and (2). Then, after two integral, time domain displacement is obtained and can be used to recalculate the magnetic force. Detailed Simulink model is shown in the red box in Figure S6. The parameters used in the calculation are listed in Table S1.

Based on the movement equation $D(t)$, electric output of the TENG can also be calculated. Through the quasi-infinitely large plane model and Kirchhoff's law, the current can be expressed as:

$$I(t) = \frac{V(t)}{R_L} = \frac{[Q_0 - \Delta Q(t)]D(t)}{A\varepsilon_0 R_L} - \frac{\Delta Q(t)d_1}{A\varepsilon_1\varepsilon_0 R_L} - \frac{\Delta Q(t)d_2}{A\varepsilon_2\varepsilon_0 R_L},$$

where ΔQ is the transferred charges, Q_0 is the charges on the friction surface, $D(t)$ is the movement equation, A is the area of the friction surface, R_L is the external load resistance, ε_0 is the vacuum permittivity, ε_i and d_i ($i = 1, 2$) are the relative permittivity and thickness of the two friction materials, respectively. Combined with

$$I(t) = \frac{\partial \Delta Q(t)}{\partial t},$$

an ordinary differential equation of ΔQ can be obtained as:

$$\frac{\partial \Delta Q(t)}{\partial t} = P_1 D(t) - P_2 D(t)\Delta Q(t) - P_3 \Delta Q(t),$$

where $P_1 = \frac{Q_0}{A\varepsilon_0 R_L}$, $P_2 = \frac{1}{A\varepsilon_0 R_L}$, $P_3 = \frac{d_1}{A\varepsilon_1\varepsilon_0 R_L} + \frac{d_2}{A\varepsilon_2\varepsilon_0 R_L}$. The Simulink model to slove this differential equation is shown in the blue box in Figure S6. Calculation results by the Simulink model is shown in Figure S6. By changing the tilt angle θ, different movement equations are obtained, which will affect the final time domain output voltage shown in Figure S6a. Detailed time domain displacement and output voltage at the tilt angle of 90° are shown in Figure S6b, c, respectively.

1. Roundy, S., Right, P. K. & Rabaey, J. A study of low level vibrations as a power source for wireless sensor nodes. *Comput. Commun.* **26**, 1131–1144 (2003).
2. Wang, Z. L. Self-powered nanosensors and nanosystems. *Adv. Mater.* **24**, 280–285 (2012).
3. Glynne-Jones, P., Tudor, M. J., Beeby, S. P. & White, N. M. An electromagnetic, vibration-powered generator for intelligent sensor systems. *Sens. Actuators, A* **110**, 344–349 (2004).
4. Külah, H. & Najafi, K. Energy scavenging from low-frequency vibrations by using frequency up-conversion for wireless sensor applications. *IEEE Sens. J.* **8**, 261–268 (2008).
5. Wang, X., Song, J., Liu, J. & Wang, Z. L. Direct-current nanogenerator driven by ultrasonic waves. *Science* **316**, 102–105 (2007).
6. Cha, S. M. *et al.* Sound-driven piezoelectric nanowire-based nanogenerators. *Adv. Mater.* **22**, 4726–4730 (2010).
7. Chang, C., Tran, V. H., Wang, J., Fuh, Y.-K. & Lin, L. Direct-write piezoelectric polymeric nanogenerator with high energy conversion efficiency. *Nano Lett.* **10**, 726–731 (2010).
8. Mitcheson, P. D. *et al.* MEMS electrostatic micropower generator for low frequency operation. *Sens. Actuators, A* **115**, 523–529 (2004).
9. Lo, H. & Tai, Y. C. Parylene-based electret power generators. *J. Micromech. Microeng.* **18**, 104006 (2008).
10. Fan, F. R., Tian, Z. Q. & Wang, Z. L. Flexible triboelectric generator. *Nano Energy* **1**, 328–334 (2012).
11. Wang, Z. L. Triboelectric nanogenerators as new energy technology for self-powered systems and as active mechanical and chemical sensors. *ACS Nano* **7**, 9533–9557 (2013).
12. Zhu, G. *et al.* Toward large-scale energy harvesting by a nanoparticle-enhanced triboelectric nanogenerator. *Nano Lett.* **2013**(13), 847–853.
13. Fan, F. R. *et al.* Transparent triboelectric nanogenerators and self-powered pressure sensors based on micropatterned plastic films. *Nano Lett.* **12**, 3109–3114 (2012).
14. Tang, W., Meng, B. & Zhang, H. Investigation of power generation based on stacked triboelectric nanogenerator. *Nano Energy* **2**, 1164–1171 (2013).
15. Yang, Y. *et al.* Human skin based triboelectric nanogenerators for harvesting biomechanical energy and as self-powered active tactile sensor system. *ACS Nano* **7**, 9213–9222 (2013).
16. Lin, Z.-H., Cheng, G., Lin, L., Lee, S. & Wang, Z. L. Water-solid surface contact electrification and its use for harvesting liquid-wave energy. *Angew. Chem. Int. Ed.* **52**, 12545–12549 (2013).
17. Wang, S., Long, L. & Wang, Z. L. Nanoscale triboelectric-effect-enabled energy conversion for sustainably powering portable electronics. *Nano Lett.* **12**, 6339–6346 (2012).
18. Zhang, X. S. *et al.* Frequency-Multiplication High-Output Triboelectric Nanogenerator for Sustainably Powering Biomedical Microsystems. *Nano Lett.* **13**, 1168–1172 (2013).
19. Yang, W. *et al.* Harvesting energy from the natural vibration of human walking. *ACS Nano* **2013**, DOI: 10.1021/nn405175z.
20. Chen, J. *et al.* Harmonic-Resonator-Based Triboelectric Nanogenerator as a Sustainable Power Source and a Self-Powered Active Vibration Sensor. *Adv. Mater.* **25**, 6094–6099 (2013).
21. Lin, Z. H. *et al.* Water-solid surface contact electrification and its use for harvesting liquid wave energy. *Angew. Chem. Int. Ed.* **52**, 5065–5069 (2013).
22. Niu, S. *et al.* Theoretical study of contact-mode triboelectric nanogenerators as an effective power source. *Energy Environ. Sci.* **6**, 3576–3583 (2013).
23. Wang, S. *et al.* Sliding-triboelectric nanogenerators based on in-plane charge-separation mechanism. *Nano Lett.* **13**, 2226–2233 (2013).
24. Niu, S. *et al.* Theory of sliding-mode triboelectric nanogenerators. *Adv. Mater.* **25**, 6184–6193 (2013).
25. Yang, Y. *et al.* Single-electrode-based sliding triboelectric nanogenerator for self-powered displacement vector sensor] system. *ACS Nano* **7**, 7342–7351 (2013).
26. Meng, B. *et al.* A transparent single-friction-surface triboelectric generator and self-powered touch sensor. *Energy Environ. Sci.* **6**, 3235–3240 (2013).
27. Han, M. D. *et al.* Low-frequency wide-band hybrid energy harvester based on piezoelectric and triboelectric mechanism. *Sci. China Tech. Sci.* **56**, 1835–1841 (2013).
28. Han, M. D. *et al.* r-Shaped hybrid nanogenerator with enhanced piezoelectricity. *ACS Nano* **7**, 8554–8560 (2013).
29. Yang, Y. *et al.* Hybrid energy cell for degradation of methyl orange by self-powered electrocatalytic oxidation. *Nano Lett.* **13**, 803–808 (2013).
30. Diaz, A. F. & Felix-Navarro, R. M. A semi-quantitative tribo-electric series for polymeric materials: the influence of chemical structure and properties. *J. Electrost.* **62**, 277–290 (2004).
31. Schill Jr, R. A. General relation for the vector magnetic field of a circular current loop: A closer look. *IEEE Trans. Magn.* **39**, 961–967 (2003).
32. Jung, H., Kim, C. J. & Kong, S. H. An optimized MEMS-based electrolytic tilt sensor. *Sens. Actuators, A* **139**, 23–30 (2007).
33. Olaru, R. & Dragoi, D. D. Inductive tilt sensor with magnets and magnetic fluid. *Sens. Actuators, A* **120**, 424–428 (2005).
34. Guan, B. O., Tam, H. Y. & Liu, S. Y. Temperature-independent fiber bragg grating tilt sensor. *IEEE Photonics Technol. Lett.* **16**, 224–226 (2004).

Acknowledgments

www.nature.com/**scientificreports**

Author contributions

M.H., X.S.Z. and H.Z. conceived the idea and designed the experiment. M.H. and X.S. performed the measurements and analyzed the data. B.M. did the fabrication work. W.L. set up the test platform. M.H., X.S.Z. and H.Z. wrote the paper and all authors provided feedback.

Additional information

Supplementary information accompanies this paper at http://www.nature.com/scientificreports

Competing financial interests: The authors declare no competing financial interests.